Control surface interaction effects

of the Active Aeroelastic Wing wind tunnel model

Jennifer Heeg*
NASA Langley Research Center, Hampton, Virginia, 23661

This paper presents results from testing the Active Aeroelastic Wing wind tunnel model in NASA Langley's Transonic Dynamics Tunnel. The wind tunnel test provided an opportunity to study aeroelastic system behavior under combined control surface deflections, testing for control surface interaction effects. Control surface interactions were observed in both static control surface actuation testing and dynamic control surface oscillation testing. The primary method of evaluating interactions was examination of the goodness of the linear superposition assumptions. Responses produced by independently actuating single control surfaces were combined and compared with those produced by simultaneously actuating and oscillating multiple control surfaces. Adjustments to the data were required to isolate the control surface influences. Using dynamic data, the task increases, as both the amplitude and phase have to be considered in the data corrections. The goodness of static linear superposition was examined and analysis of variance was used to evaluate significant factors influencing that goodness. The dynamic data showed interaction effects in both the aerodynamic measurements and the structural measurements.

Nomenclature

G	=	transfer function
G^*	=	transfer function resulting from linear superposition
$\overline{G}$	=	input-output relationship associated with combined actuation, computed relative to a reference input
u	=	control surface input, e.g. deflection of the trailing edge inboard control surface
y	=	output response of the model, e.g. lift coefficient or wing root bending moment
U	=	static control surface input
Y	=	static output response of the model
ΔU	=	static input angle correction
ΔY	=	static output correction term
C_{Y_U}	=	linear derivative of static output, Y, with respect to static input, U
α	=	significance level for analysis of variance
α	=	angle of attack
δ	=	control surface deflection
(A)	=	data set where control surface 1 is active
(B)	=	data set where control surface 2 is active
(C)	=	data set where control surface 3 is active
(D)	=	data set where control surface 4 is active
(Z)	=	data set where multiple control surfaces are active
(0)	=	data set where no control surfaces are active; baseline static data set
Subscripts		
1,2,3, or 4	=	associated with the i^{th} input
R	=	raw data set; static data set, prior to correction with baseline data
TEO	=	Trailing Edge Outboard control surface deflection
LEO	=	Leading Edge Outboard control surface deflection

* Research engineer, Aeroelasticity Branch, Mail Stop 340, Senior Member AIAA

Superscripts, and overscores

*	=	associated with linear superposition of results
ˇ	=	nominal or target deflection angle

I. Introduction

THE Active Aeroelastic Wing (AAW) program investigated improvements available by considering aeroelasticity in a beneficial light, rather than as a detriment to vehicle performance and stability[1]. Flight testing, wind tunnel testing and analyses were performed and reported in the literature[2,3,4,5]. The wind tunnel testing was conducted in NASA Langley's Transonic Dynamics Tunnel (TDT) in 2004[6], using a statically aeroelastically scaled wind tunnel model. The wind tunnel test provided an opportunity to study aeroelastic system behavior under combined control surface deflections, testing for control surface interaction effects. Interaction effects are addressed primarily through examining the goodness of linear superposition assumption. Both static and dynamic responses are examined.

Several advanced vehicle concepts utilize multiple control surfaces, including the Active Flexible Wing[7,8], the Blended Wing Body[9], and the X-33[10]. Research concepts such as microflap actuators[11] and distributed piezoelectric actuators[12] involve even larger arrays of control devices. Control surface interaction effects are present to some extent whenever multiple control surfaces are utilized together. *How important are these interactions?* The answer likely depends upon the flight condition and vehicle configuration. The current study examines control surface interactions in the transonic range using a wing that is highly flexible for a fighter-class vehicle.

Linear superposition of responses[13] is often applied in generating models for control law design and for simulation[14,15]. This paper explores the validity of the linear superposition process for static responses, considering control surfaces that are aligned with each other relative to the flow- that is, a leading edge and a trailing edge control surface with approximately the same spanwise location and extent. *Can the rolling moment produced by a leading edge deflection and the rolling moment produced by a trailing edge deflection be added together, producing the same rolling moment as if they had both been physically deflected at the same time?* Analysis of the static control surface deflection data says yes, under some conditions, with some parameter sets. The issue expands: *What parameters affect the validity of the superposition assumption?* To address this, the data was organized into a design of experiments framework[16,17] and examined through ANalysis Of VAriances (ANOVA)[18,19].

Dynamic data is also examined in this paper for control surface interactions. Simultaneous control surface oscillations were examined for tandem and adjacent pairings, as well as all control surfaces acting simultaneously. The combined dynamic responses were examined as functions of frequency and phasing of the control surface positions. The data is examined for linear superposition prediction of control surface authority, and for the influence of control surface phase on the model responses.

II. Wind Tunnel Model

The AAW wind-tunnel model is a 26% geometrically scaled right half-span representation of an F/A-18A. Figure 1 is a photo of the model installed in the TDT test section. A contoured aluminum core simulates the main wing stiffness of the AAW flight vehicle while a balsa wood covering provides the proper airfoil shape. The model has four control surfaces, a leading edge outboard (LEO) control surface, a leading edge inboard (LEI) control

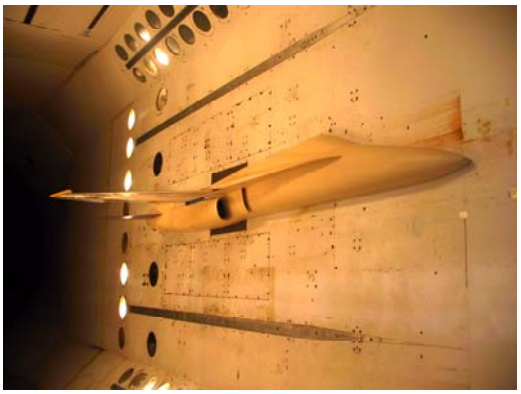

Figure 1. AAW wind tunnel mounted, mounted in the TDT test section

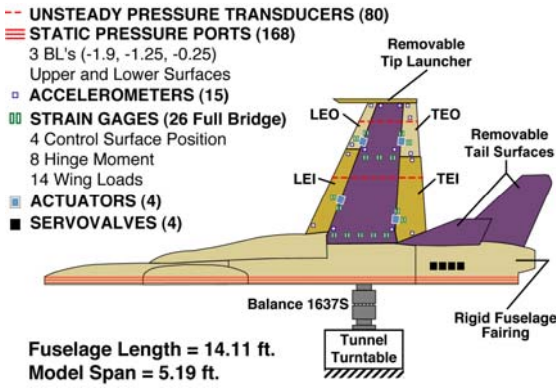

Figure 2. Schematic Planform of AAW wind tunnel model and instrumentation

surface, a trailing edge outboard (TEO) control surface, and a trailing edge inboard (TEI) control surface. The control surfaces are attached to the main wing structure through control surface flexures and vane-type hydraulic actuators.

Figure 2 shows a schematic of the AAW model configuration and instrumentation layout. The model is mounted to the tunnel sidewall turntable through a five-component balance used for measuring aerodynamic loads. Two rows of 40 pressure orifices are installed in the wing at roughly 53.8% and 89.6% of the model semispan. These ports are instrumented with unsteady pressure transducers. A combination of 14 bending and torsion strain gages were applied to the main wing at the root and 2/3-span (near the wing fold span station of an F/A-18) to determine the loads on the model. The control surface position sensors consist of small torsion beam flexures instrumented with torsion strain gages and attached to each actuator to measure the control surface deflection angles.

III. Test Conditions & Data Sets

The NASA Langley Transonic Dynamics Tunnel (TDT) is a closed-circuit reduced-pressure tunnel located at sea level. The test data used in the current studies was produced by testing in a heavy gas test medium, R134a. The conditions at which the wind tunnel measurements were made for control surface interaction studies are designated as test condition matrix C. Other data sets acquired during this wind tunnel test are detailed in previous publications[4, 6]. Those data sets were used to match analyses and flight test points, investigate reversal and divergence, and investigate transonic similarity.

The control surface interaction test condition matrix is divided into static data acquisition test conditions and dynamic data acquisition test conditions. These test conditions are shown in figure 3, overlaid with the TDT test envelope for R134a.

For each static data test point, model responses were acquired for independent static deflection of the leading edge outboard and trailing edge outboard control surfaces, and combined actuation of those surfaces. At the test conditions, relative positioning, or phasing, of the control surfaces was varied. Angle of attack also varied among the conditions.

For each dynamic data test point, each of the four control surfaces was oscillated individually, at several discrete frequencies. Combinations of adjacent and tandem control surfaces were also investigated at several frequencies. The relative phasing of the control surfaces was also varied.

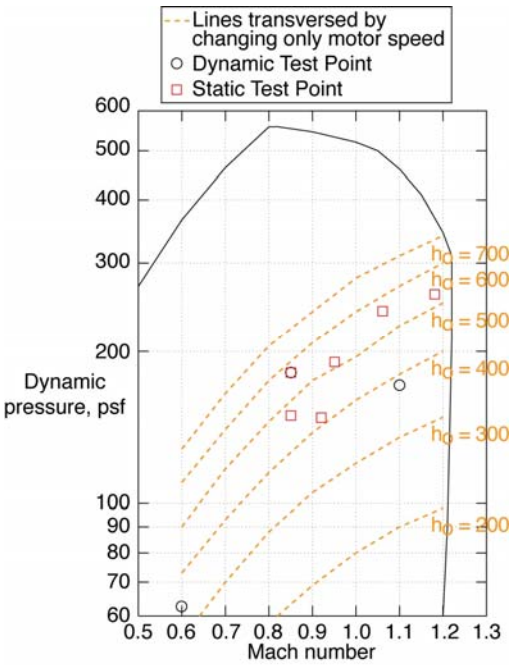

Figure 3. Test matrices and TDT test envelope in R134a

IV. Static Control Surface Interaction Studies

The static control surface interaction issue is examined first. The fundamental question is whether the responses produced by individually deflected control surfaces can be summed to accurately represent the response produced when deflecting them simultaneously. More precisely, is the process of linear superposition of individual control surfaces valid for a flexible wing, particularly when operating in the transonic flight regime?

The static interaction studies are limited to the combination of leading edge outboard and trailing edge outboard control surface effects. In this study, model responses produced by independent actuation of the leading edge control surface and independent actuation of the trailing edge control surface are combined. The combined response is compared to the response produced by simultaneously commanding both control surfaces. The difference in these responses shows the degree to which the control surfaces interact or interfere with each other, and the extent to which linear superposition of the responses exists. Loads from both the balance and the wing strain gauges are considered in this study. Once the individual and simultaneous responses are acquired, ANOVA is employed to assess which, if any, of several factors significantly influences the quality of the linear superposition of the responses.

A. Control Surface Phase Relationships

Combining the static control surface deflections in various ways produces different amounts of wing twist, and different flow fields. To investigate the potentially different characteristics, data was acquired for four combinations of control surface relative positions, or phasing. Positive control deflections are defined by the free edge of the surface deflected downward. Figure 4 shows the four combinations of static control deflections used in this study. The first data set has the LEO deflected upward and the TEO deflected downward. In the second they are both deflected upward; in the third LEO is down and TEO is up; and in the fourth both are deflected downward. Note that data set 1 corresponds to maximum wing twist, nose up, and data set 3 corresponds to maximum wing twist, nose down.

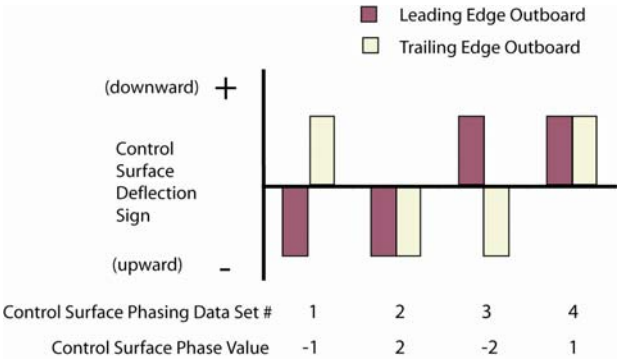

Figure 4. Control surface phasing data set definitions

B. Computation of Linear Superposition and Simultaneous Actuation Responses

Experimental data sets from individually deflected control surfaces are combined using linear superposition and compared to responses measured when those same control surfaces are simultaneously deflected. To isolate the control surface effects, several corrections to the raw data must be incorporated. These include correcting for nonsymmetries, angle of attack and small differences in model angles and deflections that occur between the data sets being compared. To accomplish this, four data sets are required: **Z)** simultaneously actuated leading and trailing edge control surfaces, commanded to target deflection angles, with the angle of attack commanded to a target value; **0)** the baseline data set, with control surfaces commanded to zero and the angle of attack commanded to the target value; **A)** trailing edge control surface and angle of attack commanded to their target values; and **B)** trailing edge control surface and angle of attack commanded to their target values. Table 1 summarizes these data sets.

Table 1 Static deflection data sets

		Data Set			
	Description	Simultaneous Deflection	Baseline	TEO only Commanded Deflection	LEO only Commanded Deflection
	Designation	**Z**	**0**	**A**	**B**
Target or Nominal Values of Deflection Angles	Angle of attack	$\breve{\alpha}$	$\breve{\alpha}$	$\breve{\alpha}$	$\breve{\alpha}$
	TEO deflection	$\breve{\delta}_{TEO}$	0	$\breve{\delta}_{TEO}$	0
	LEO deflection	$\breve{\delta}_{LEO}$	0	0	$\breve{\delta}_{LEO}$

A sample of the data sets to be combined is shown in figure 5. The data was obtained at Mach 0.85, 182 psf dynamic pressure, at a nominal angle of attack of -1 degree. The angles shown are the actual angles measured on the model- note that the angles are not precisely the same for all of the data sets. This necessitates making small corrections using additional information, discussed subsequently.

The first adjustment to the data is made using the baseline responses. Each of the other three data sets is corrected by

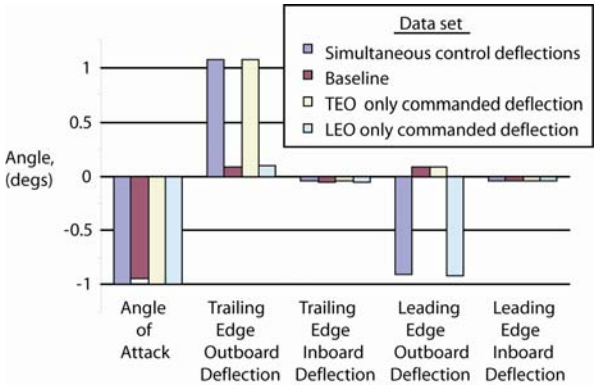

Figure 5. Measured deflection angles for static data sets, Mach 0.85, q 182 psf

subtracting off the baseline data responses. The variable Y generically represents each of the static output responses under consideration. The subscript R indicates the raw measured data. The parenthetical designations show which data set is used: Z, 0, A or B. Correcting the simultaneous actuation responses by subtracting out the baseline:

$$Y(Z) = Y_R(Z) - Y(0) \tag{1}$$

Likewise, correcting the data set with only the TEO commanded to the target value,

$$Y(A) = Y_R(A) - Y(0) \tag{2}$$

and correcting the data set with only the LEO commanded to the target value

$$Y(B) = Y_R(B) - Y(0) \tag{3}$$

Figure 6a shows an example of the results of this correction process, using the rolling moment response. The raw data sets and the results of subtracting off the baseline data are shown by the first six bars on the graph. Failure to subtract the baseline contribution to the responses can lead to significant errors due to nonsymmetries (e.g. C_{L_0} contribution to the lift coefficient) and angle of attack contributions. This is readily observed from the results shown- adding the leading edge and trailing edge raw data together would produce a value that is significantly larger than the simultaneous actuation result. The majority of the difference between the results would then be due to the angle of attack contribution being doubled for the linear superposition result. The responses are significantly reduced once the baseline is removed; figure 6b presents the information rescaled, without the raw data.

The trailing and leading edge control surface responses, shown by blue and yellow bars respectively, are added together, illustrated by the light green bar on the chart. Recall from figure 5 that the model angles for each data set are not precisely the same. Small differences, particularly in the angle of attack, can exert large influences on the superimposed result. Thus, a correction was applied in generating the linear superposition result.

$$Y^*(Z) = Y(A) + Y(B) - \Delta Y \tag{4}$$

The correction term was generated using linear stability and control derivatives computed in reference 6. The previously computed derivatives assumed a linear least squares model applied at each test point, and utilized control surface deflections of less than 1°. The derivatives of a static output response, Y, are organized into a row vector.

$$\lfloor C_{Y_U} \rfloor = \left\lfloor \frac{\partial Y}{\partial \alpha} \quad \frac{\partial Y}{\partial U_1} \quad \frac{\partial Y}{\partial U_2} \quad \frac{\partial Y}{\partial U_3} \quad \frac{\partial Y}{\partial U_4} \right\rfloor \tag{5}$$

An angle correction vector is formed using the four previously described data sets:

$$\{\Delta U\} = \begin{Bmatrix} \alpha(A) + \alpha(B) - \alpha(Z) - \alpha(0) \\ U_1(A) + U_1(B) - U_1(Z) - U_1(0) \\ U_2(A) + U_2(B) - U_2(Z) - U_2(0) \\ U_3(A) + U_3(B) - U_3(Z) - U_3(0) \\ U_4(A) + U_4(B) - U_4(Z) - U_4(0) \end{Bmatrix} \tag{6}$$

The correction term is then formed:

$$\Delta Y = \lfloor C_{Y_U} \rfloor \{\Delta U\} \tag{7}$$

Note that the above adjustments to the angles result in both the simultaneous actuation results and the linear superposition results being computed for model angles formed by the simultaneous deflection set minus the baseline data set.

$$\alpha(Z) = \alpha^*(Z) = \alpha_R(Z) - \alpha(0) \tag{8}$$

Linear superposition of the trailing and leading edge control surface responses, adjusted via the linear control derivatives to account for the small disagreements among the angles, are illustrated by the darker green bar. The data sets shown by the first and last bars of figure 6b can now be compared to see the difference between the

simultaneous actuation response and the linear superposition.

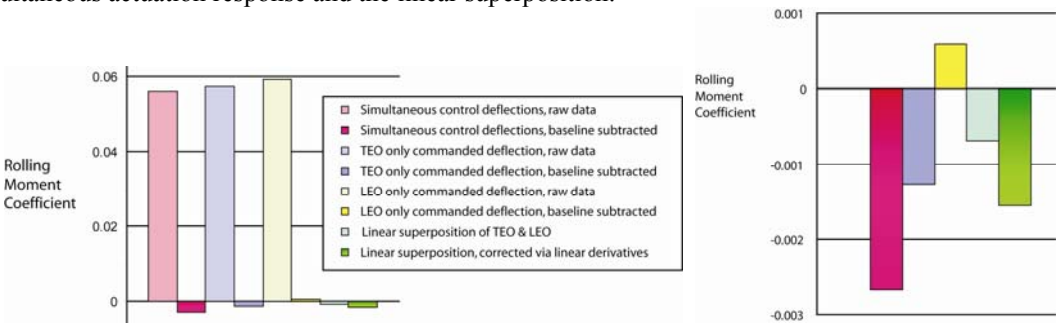

a) including raw data **b) excluding raw data**

Figure 6. Rolling moment coefficient at Mach 0.85, 182 psf dynamic pressure

C. Comparison of Data Sets

The process outlined above was applied to data obtained for forty-one combinations of test conditions and model parameters. Several example results are shown in figure 7. Figure 7 presents three model responses: lift coefficient, rolling moment coefficient and wing root bending moment. These correspond, in order, to the three columns of plots shown. Each row of plots corresponds to a combination of wind tunnel condition, angle of attack and control surface deflection amplitude; the values of these variables for each row are given to the left of the plots. Note that the wind tunnel condition is only specified by the Mach number in this table, but actually represents changing Mach number and dynamic pressure.

Each of the subplots contains several data sets, corresponding to the different control surface phasings. The phase data set number is shown on the x-axis (abscissa). These correspond to the definitions given in figure 4. For each phase relationship, there are two vertical bars; the first bar (orange) shows the linear superposition result after all adjustments have been made and the second bar (blue) shows the simultaneous actuation result after all adjustments have been made. The vertical scales are not consistent from one subplot to another; they have been removed for visual clarity.

Examining the first row of subplots, this data was acquired at Mach 0.85, -1 degree angle of attack, with all of the control surface deflections being commanded to 1 degree amplitude. The first subplot shows the lift coefficient. The first two bars show the lift coefficient when the leading edge control surface is deflected upward and the trailing edge control surface is deflected downward. The linear superposition result is larger than the simultaneous actuation result. In this particular case, applying linear superposition would lead to a 32% over prediction of the lift coefficient due to control surface deflections.

Examining the subplots shows that some test conditions produce very good agreement between linear superposition and simultaneous actuation, while others produce poor agreement. The quality of each comparison was evaluated through a goodness metric, which was calculated in this study by computing the percent error relative to each of the quantities- linear superposition result and simultaneous actuation result- and taking the minimum of these two values. Histogram data was generated for each of the measured responses, grouping the goodness metrics into 5 bins, shown in figure 8. Each of the shades of grey represents a different histogram bin. The white boxes show the number of results having errors less than 10%. As the shade of grey gets darker, increased error is indicated. Each of the boxes in a column represents one of the forty-one cases. Examining the lift and pitching moment coefficients, more than half of the cases have less than 10% error due to linear superposition. The wing torsion moments were not well captured by linear superposition, with more than 50% of the cases considered having greater than 70% error. The other loads had results lying between these extremes.

The torsion moments produced by combined control surface actuation are shown to be ill-represented by linear superposition. Before reducing the data, it was suspected that the outboard moments, whose sensors are in the local vicinity of the control surface being actuated, would be much more poorly represented by linear superposition than those at the wing root. The results, however, indicate only a slight tendency towards this characteristic. This insensitivity is potentially due to an extensive study that was done to optimize the placement, orientation and calibration of the strain gauges used to produce the wing loads.

Because there is great variation in how well the linear superposition result represents the simultaneous actuation result, the question arises: *What parameters affect the validity of the superposition assumption?* To address this, the data was organized into a design of experiments framework and examined through analysis of variances.

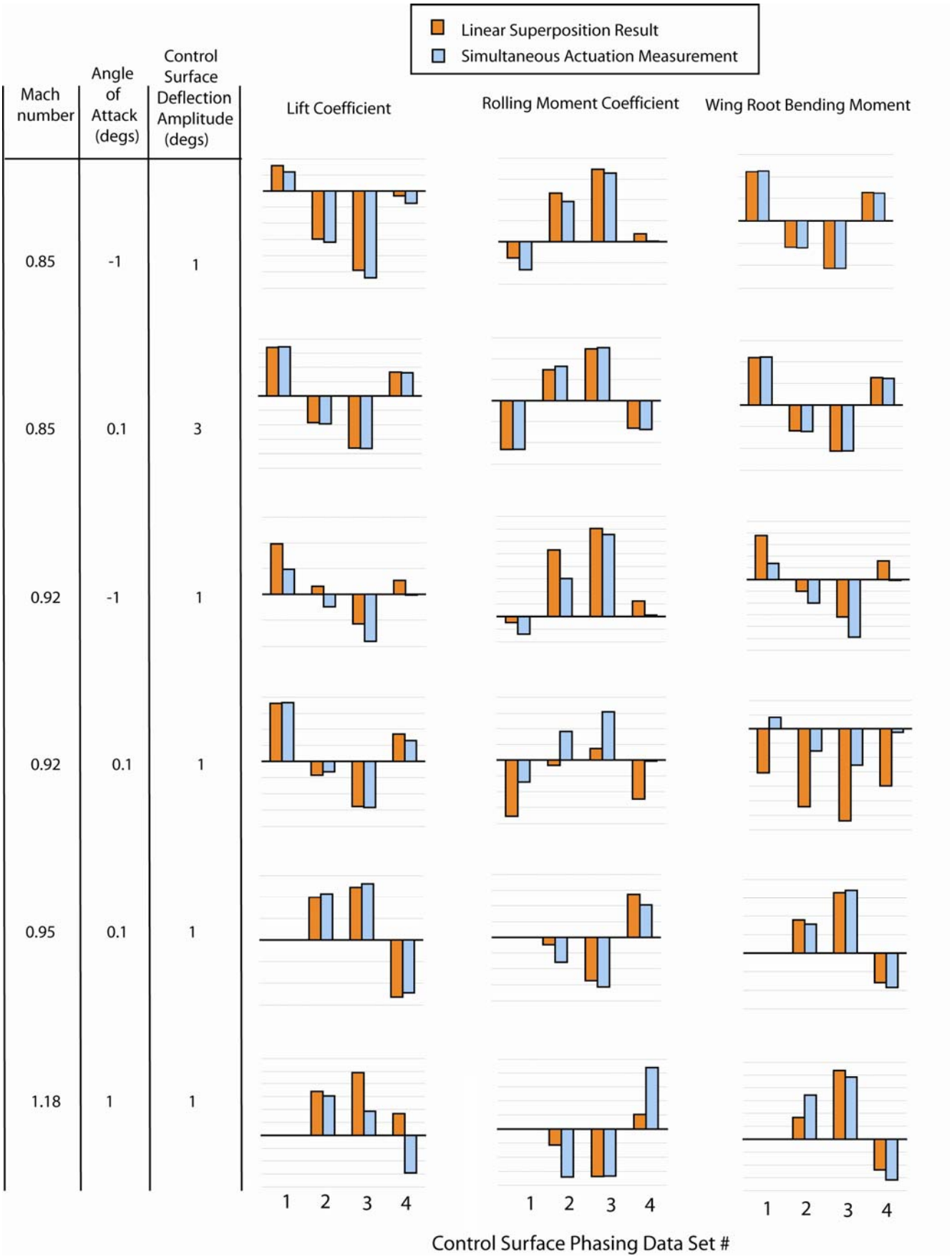

Figure 7. Comparison of linear superposition and simultaneous actuation results

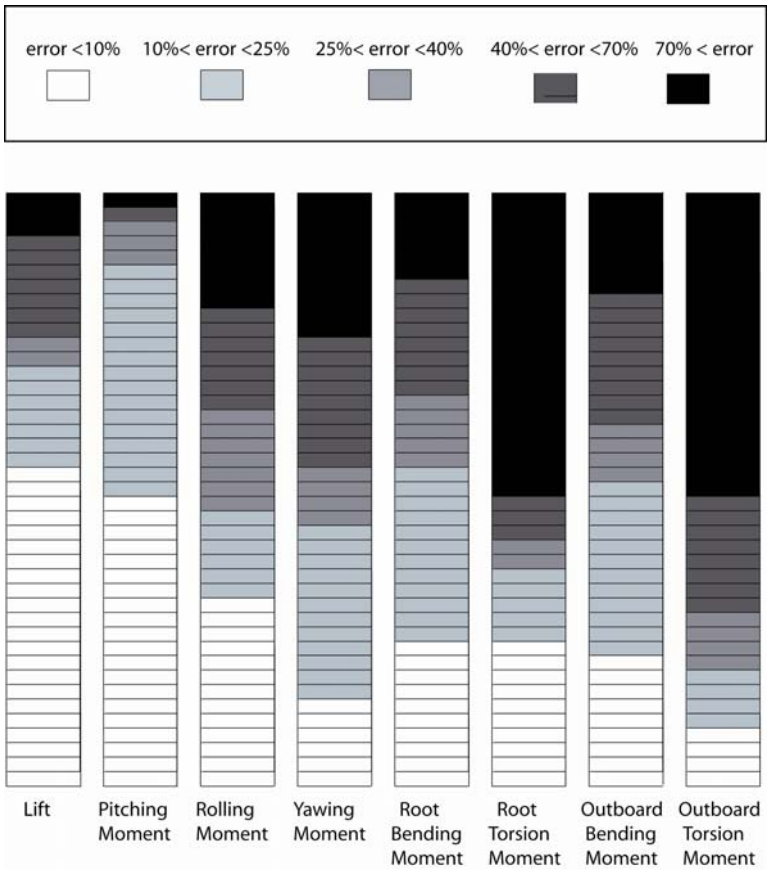

Figure 8. Percent error due to linear superposition assumption, for static data sets

D. Analysis of Variance

Analysis of variance (ANOVA) is a statistical method for analyzing data, evaluating factors for statistical significance. There are long histories of using ANOVA in production process characterization, sociology and psychology. In the current study, ANOVA is used to determine which factors significantly affect the difference between the linear superposition result and the simultaneous actuation data. The ANOVA results of this study do not indicate whether linear superposition is valid, only whether a given factor significantly affects the error. In this particular ANOVA, a fixed effects statistical model is employed. Thus the values for each of the factors are limited to a pre-selected set of values, referred to as levels or treatments. Details on ANOVA and fixed effects models and ANOVA can be found in references 16 and 18.

1. Methodology

The analysis of variance utilized in this study employs the statistical f-test to determine whether there exists a significant difference among the mean values of different data treatments or levels of a factor. The null hypothesis assumes that there is no difference among the levels for a factor. A test statistic is computed for each factor. If the null hypothesis is accepted, there is an implication that no relation exists between the factor levels and the response. Critical values associated with significance level, α, are compared to the calculated test statistic. When the test statistic exceeds the critical value, the null hypothesis is rejected with $(1-\alpha)*100\%$ confidence. A value of $\alpha = 0.05$ implies that the null hypothesis is rejected 5% of the time when it is in fact true; the factor is considered significant with 95% confidence. Whether a factor is deemed significant is a subjective evaluation, as the significance level has to be chosen. Standard practice in many fields is to use a significance level $\alpha=0.05$. For this study, that standard has been relaxed.

2. Contributing Factors & Goodness Metrics

Five factors were analyzed for potential significance; Mach number, angle of attack, amplitude of control surface deflection, control surface phasing and slippage of the TEI control surface. These factors and the associated

levels are summarized in Table 2. The meaning of the control surface phasings was given previously in figure 4. Slippage of the trailing edge inboard control surface occurred during an early phase of the wind tunnel test. Hydraulic actuators were utilized to deflect the control surfaces and to hold them in place. The actuator that permitted the TEI slippage was subsequently repaired, but the test points used in this study were not repeated after the repair. The value of slippage is denoted as 1 if it slipped, and -1 if it did not slip.

Table 2 ANOVA factors

Factor	# of levels	Levels or Treatments
Amplitude of control deflection (degs)	2	1; 3
Slippage of trailing edge inboard surface	2	-1; 1
Angle of attack (degs)	3	-1; 0.1; 1
Control surface phasing	4	-2; -1; 1; 2
Mach number	5	0.85; 0.92; 0.95; 1.06; 1.18

The goodness metric described in the preceding section was the primary data used in the analysis of variance. This metric was chosen after considering percent difference, and percent error relative to each of the compared quantities. In all three of these cases, outlier data was being created due solely to the reference or denominator value lying near zero, rather than creating outlier data which truly represented large and significant differences between the quantities. It was also not desirable to use the raw differences because different parameter values naturally produce larger responses and bias the results substantially. A good set of ANOVA data is normally distributed and has constant mean and standard deviation. The chosen goodness metric- the minimum of the %errors- had the best properties relative to the desired ANOVA traits.

3. Sample results

For each of the output responses, a separate ANOVA study was performed. For each study, analysis was performed to assess the significance of each of the five factors. The angle of attack factor results from the analysis of the rolling moment coefficient are shown in figure 9. The horizontal line shows the test statistic calculated from the rolling moment data. The curve show the critical value plotted against the significance level, α. Because the factors have different numbers of levels, the critical value curves associated with the factors differ. The significance level for a given factor is determined by finding the point at which that factor's test statistic crosses the critical value curve. For the angle of attack in figure 9, the vertical line indicates the crossing point at a significance value of 0.25. This indicates that the angle of attack has a significant impact on the goodness metric with approximately 75% confidence.

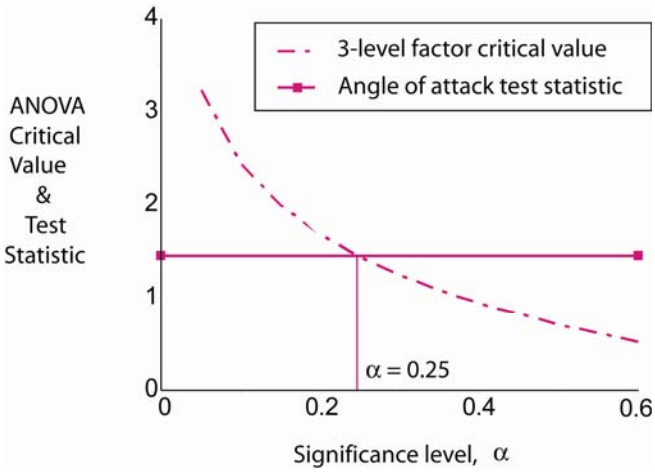

Figure 9. Analysis of variance results, angle of attack for rolling moment coefficient

4. Summary of results

For each of the factors, for each of the loads, the significance levels were computed and converted to percent confidence values. High values indicate that the factor significantly influences the validity of linear superposition. The results are summarized in figure 10. Amplitude of control surface deflection is shown to be insignificant for most of the loads. Angle of attack is the most significant factor when all loads are considered. Mach number is shown to be moderately significant for most of the loads. The goodness metric for lift coefficient is not likely to be significantly influenced by any of the factors considered. The pitching moment goodness metric, on the other hand, is significantly influenced by all of the factors except amplitude. Grouping the balance loads together and summing the confidence levels, the factors are ordered from most significant to least significant: TEI slippage, angle of attack, Mach number, control surface phasing and amplitude. Grouping the wing loads together, the factors ordered by overall significance are angle of attack, TEI slippage, Mach number, control surface amplitude and phasing.

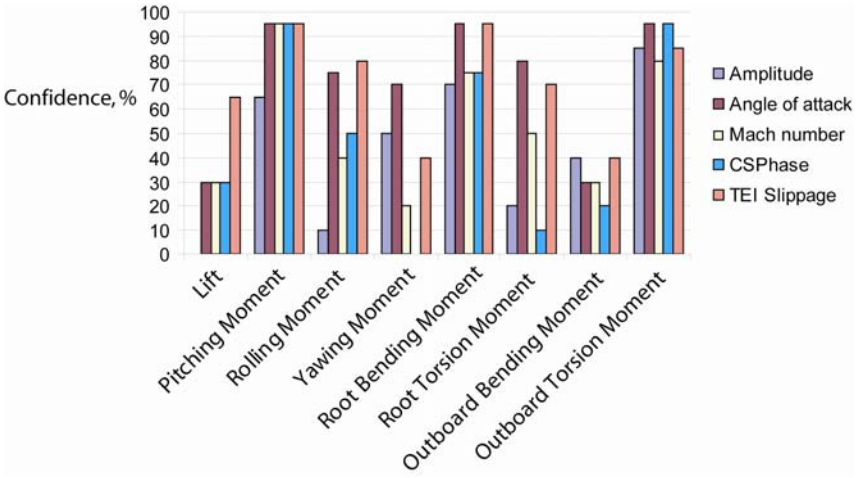

Figure 10. ANOVA results

E. Interpretation of results

Interpreting the results requires that figures 8 and 11 be considered together. Recall that the lightness of the boxes in figure 8 shows the goodness of the superposition assumption. Figure 11 shows which factors contribute to the variation of the shades of grey seen in figure 8.

The amplitude was not shown to be a significant factor in the goodness of the linear superposition process, except for the outboard torsion moment. Recall that the linear superposition result was formed by independent deflections at the appropriate amplitude. This result says nothing about the validity of linearity of responses as functions of control surface deflection amplitude. Also, the range of deflections considered was +/- 3º. Larger deflection ranges may indicate amplitude significance as the aerodynamic response becomes more complex.

The lift coefficient results are generally well-captured by linear superposition. The ANOVA results do not point to any of the considered factors as the responsible cause of the variation, with a high degree of confidence. Slippage of the TEI control surface was shown to be the most significant factor affecting lift, but the confidence is little greater than a coin flip. This points to the source of the variance being either random or assignable to a parameter that was not identified in the analysis.

The pitching moment results exhibit the lowest effect of control surface interaction, shown by good agreement of the linear superposition results and the simultaneous actuation results. The ANOVA results show that all factors considered, except amplitude, significantly influence the degree of the validity. However, since the range of goodness of the results is very narrow, the ANOVA pitching moment result offers little information.

The interaction of the control surface effects in producing the torsion moments was very high; the agreement between linear superposition and simultaneous actuation was poor. The ANOVA results show that all factors were significant for the torsion moments. The variation in the quality of the comparison is assignable to all of these parameters, however, because the quality of the comparison is uniformly poor, this information is of little value.

V. Dynamic Control Surface Interaction Studies

Similar to the goal pursued using the static data, dynamic data was analyzed for interaction effects. For each dynamic actuation data set, an oscillatory command at a single frequency was applied to either an individual control surface or simultaneously to multiple control surfaces. When multiple control surfaces were actuated, they were driven at identical frequencies and the phasing between them maintained at a constant value. Separate data sets were acquired for 3 frequencies and 7 to 8 phase relationships for several control surface combinations. Multiple control surface data sets included all adjacent pairings (TEI and TEO; LEI and LEO) and tandem pairings (TEI and LEI; TEO and LEO). All control surfaces were also simultaneously actuated, with the leading edge surfaces phased together and the trailing edge surfaces phased together.

The dynamic actuation data was analyzed in the frequency domain. This analysis was accomplished by computing the transfer function relationships- magnitude and phase- at the frequency of the forced oscillation. Balance loads and wing loads were analyzed in this manner. The frequency-domain representations of the responses

were then processed in a manner similar to the static data analysis- individual actuation responses are combined and compared to simultaneous actuation responses. This data is examined both in-phase and for phase-dependent trends.

A. Data sets

Simultaneous actuation of multiple control surfaces was not an automated test procedure. Thus, the simultaneous control surface deflections input simultaneously were dissimilar in magnitude and imprecise in phase offset. An illustration of this is shown in figure 11. In this data set, all control surfaces were oscillated with an in-phase 5 Hz command. For each frequency at each test condition for each set of control surfaces, time history data was acquired at 7 or 8 relative phase angles. Figure 12 shows the case where the leading edge control surfaces were oscillated as a pair and the trailing edge control surfaces were oscillated as a pair. The relative phasing between these pairs was varied for each of the data sets obtained.

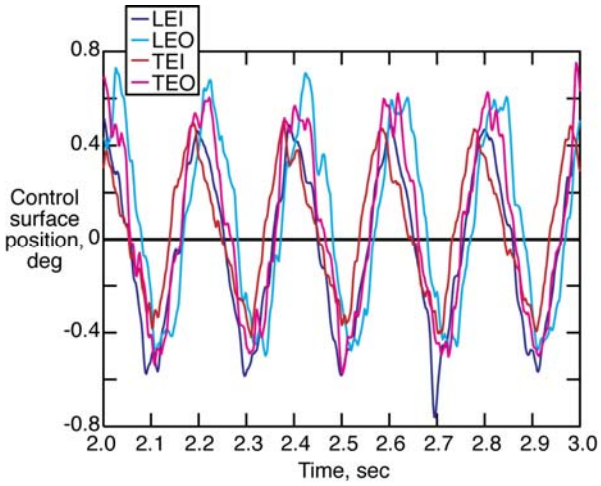

Figure 11. In phase control surface deflections

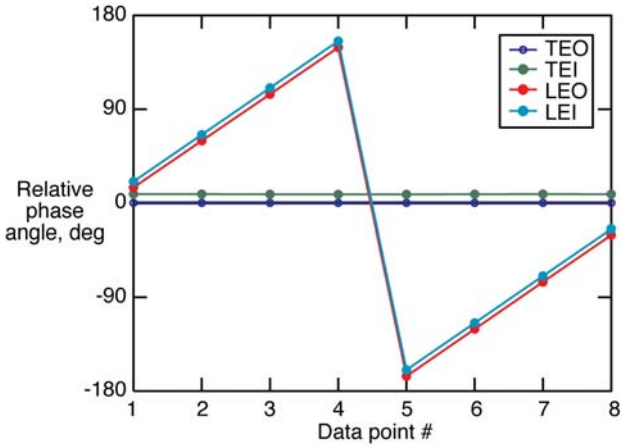

Figure 12. Phase angles for simultaneous actuation of all control surfaces, Mach 0.85, 0.5 Hz oscillations

B. Linear Superposition Methodology

Because even the in-phase actuation (figure 11) could not be considered to be accurately in-phase, and the magnitude was not accurately maintained, directly combining the independently actuated responses was inadequate. The following method was used to account for these discrepancies.

Consider test point A, where control surface 1 is deflected, $u_1(A)$, and produces response y(A). The independent actuation relationship is formed:

$$y(A) = G_1 u_1(A) \longrightarrow G_1 = \frac{y(A)}{u_1(A)} \tag{9a}$$

And similarly for test conditions B, C and D where control surfaces 2, 3, and 4 are the only active control surfaces:

$$G_2 = \frac{y(B)}{u_2(B)}; \qquad G_3 = \frac{y(C)}{u_3(C)}; \qquad G_4 = \frac{y(D)}{u_4(D)} \tag{9b,c,d}$$

While test points A, B, C and D represent the independently actuated cases, test point Z represents combined actuation data where multiple control surfaces are all active. The responses are measured, y(Z), as well as the control surface deflections, u_1 through u_4. An input-output relationship due to the first input can be computed, without direct consideration of the other surfaces' contributions.

$$y(Z) = \overline{G} u_1(Z) \tag{10}$$

System identification could be used to define individual transfer function relationships using the simultaneous actuation data. These transfer functions could then be compared to G_1 through G_4. However, the identification method itself might impose suppositions of linearity or contain other limitations. To avoid these ambiguities, the independent control surface transfer functions were combined, assuming linear superposition is valid and compared to the combined actuation response.

Input u_1 is used as the reference input; the magnitudes and phasings of the deflections of the other control surfaces are found relative to the first control surface's deflection at the oscillation frequency. That is, the inputs u_2, u_3 and u_4 for a given data set, can be represented by the complex number relationship to the first input, u_1. For the combined actuation point, Z:

$$u_2 = \left(\frac{u_2(Z)}{u_1(Z)}\right) u_1; \qquad u_3 = \left(\frac{u_3(Z)}{u_1(Z)}\right) u_1; \qquad u_4 = \left(\frac{u_4(Z)}{u_1(Z)}\right) u_1 \tag{11a,b,c}$$

If linear superposition held, then the transfer functions from the independent actuation data sets could be multiplied by the inputs for the combined actuation data set, added together to give a response of the system identical to the combined actuation response. That is, assuming linear superposition, the response equivalent to that produced by the simultaneous actuation inputs is computed:

$$y^*(Z) = G_1 u_1(Z) + G_2 u_2(Z) + G_3 u_3(Z) + G_4 u_4(Z) \tag{12}$$

Using the relationships between the inputs for the combined actuation time history, (eqns 11a, b, and c),

$$y^*(Z) = \left\{ G_1 + G_2\left(\frac{u_2(Z)}{u_1(Z)}\right) + G_3\left(\frac{u_3(Z)}{u_1(Z)}\right) + G_4\left(\frac{u_4(Z)}{u_1(Z)}\right) \right\} u_1(Z) = G^* u_1(Z) \tag{13}$$

The difference between the combined actuation response, y(Z), and the linear superposition assumption response, y*(Z), can now be made by comparison of $\overline{G}$ (eqn 10) and G^* (eqn 13).

C. Balance & Wing Loads

The dynamic linear superposition responses were computed at the frequencies of oscillation, as previously described using eqns 1 through 5. These responses were then compared to the simultaneous actuation responses. Percent errors were computed for each in-phase data set. Sample results are shown in figure 14. The top row shows data at Mach 0.85; the bottom row at Mach 1.1. The first column shows lift coefficient results; the second column shows rolling moment coefficient results. All five combinations of control surfaces are shown in each subplot. The percent error due to linear superposition is plotted as a function of actuation frequency. Most trends show an increase in error as frequency increases.

Surprisingly, the largest superposition errors observed are not observable when all four control surfaces act together. The lift and rolling moment errors are largest for combining the two inboard control surfaces at 5 Hz. Although the graphs are not shown, the largest errors on pitching moment are seen when the trailing edge control surfaces are combined. Also not shown, the root moments- bending and torsion- the inboard control surfaces being combined have the largest percent errors.

In considering the outboard span station moments, it is interesting to note that the outboard control surfaces being combined generate low percentage errors for all frequencies. These control surfaces are the major producers of loads in the outboard region. The inboard control surfaces influence the outboard span station loads less directly, as they induce a different wing shape or flow field. For the outboard span station moments, the inboard control surfaces being combined have large percent errors. This might be expected since they are actually contributing much less to the outboard span station moments than the outboard control surfaces. Thus the percent errors are higher even though their contribution to generating outboard span station loads is significantly less that the outboard control surfaces.

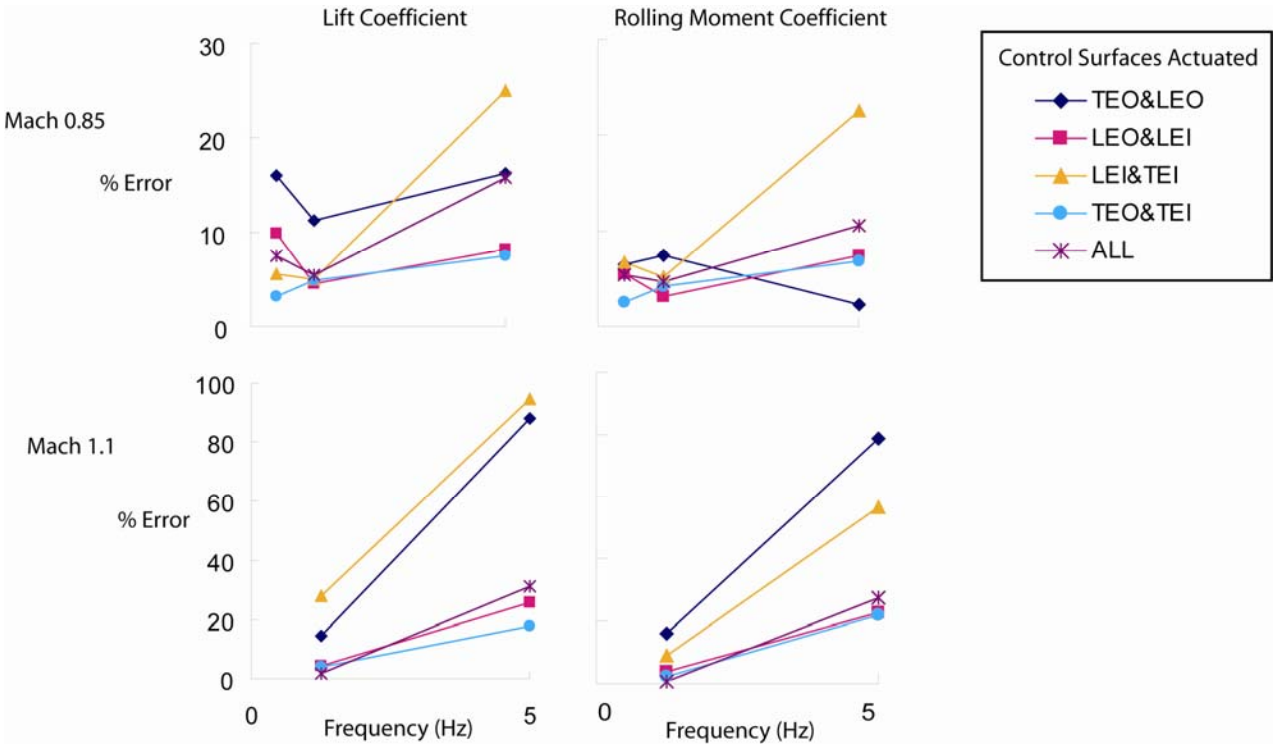

Figure 13. Percent error due to linear superposition of in-phase dynamic actuation of multiple control surfaces

D. Influence of Relative Phasing

The previous results presented data corresponding to in-phase control surface oscillation. The influence of the relative phasing between control surfaces is now examined. Control surfaces being "in phase" refers to the free edges deflected downward at the same time, moved smoothly through the deflection range and then having the free edges deflected upward at the same time. In-phase control surface deflections have 0º of relative phase between them. Out of phase control surfaces have one control surface with its free edge up while the other's free edge is down; they have 180º of relative phase between them.

For a given data point, transfer function information at the frequency of oscillation and the relative phasing of the control surfaces are computed. This is done for all of the data sets available at that test condition, for that frequency, at the different relative phase angles. The amplitude of the transfer function at a specified frequency is plotted versus the relative phase angle between the control surfaces of a given pairing, figure 14. Four such plots are shown.

Figure 14a shows the amplitude of the lift coefficient due to combined TEO and LEO actuation. The horizontal axis is the relative phase angle between TEO and LEO deflections. This data was taken at Mach 0.85. In-phase actuation produces the least amount of lift. Out of phase actuation produces the most lift. For this case, the control surfaces acting in phase produce only 50% of the lift produced when they act out of phase. The plot also shows that the linear superposition result tracks the characteristics very well, with the largest errors- although small- occurring for in phase actuation.

The data in figure 14c shows the amplitude of the rolling moment coefficient when the LEO and TEO control surfaces are oscillated at 5 Hz for Mach 1.1. Similar to the lift results, the control surfaces acting in phase produce only 15% of the rolling moment that they produce when they act out of phase. The linear superposition results indicate that there will be less rolling moment authority than is actually available when using the two surfaces together. Generally, the error caused by the superposition assumption grows as the control surfaces get more out of phase.

Figures 14 b and d show data for the same test conditions as 14 a and c, but with the trailing edge inboard and outboard control surfaces acting. A primary difference that arises when comparing these plots to the previously discussed pair is that the maximum response is achieved for in-phase actuation. Acting in-phase, they produce a lift response that is almost three times the out-of-phase response. Another difference is that the error in rolling moment coefficient due to linear superposition is largest for the in-phase actuation.

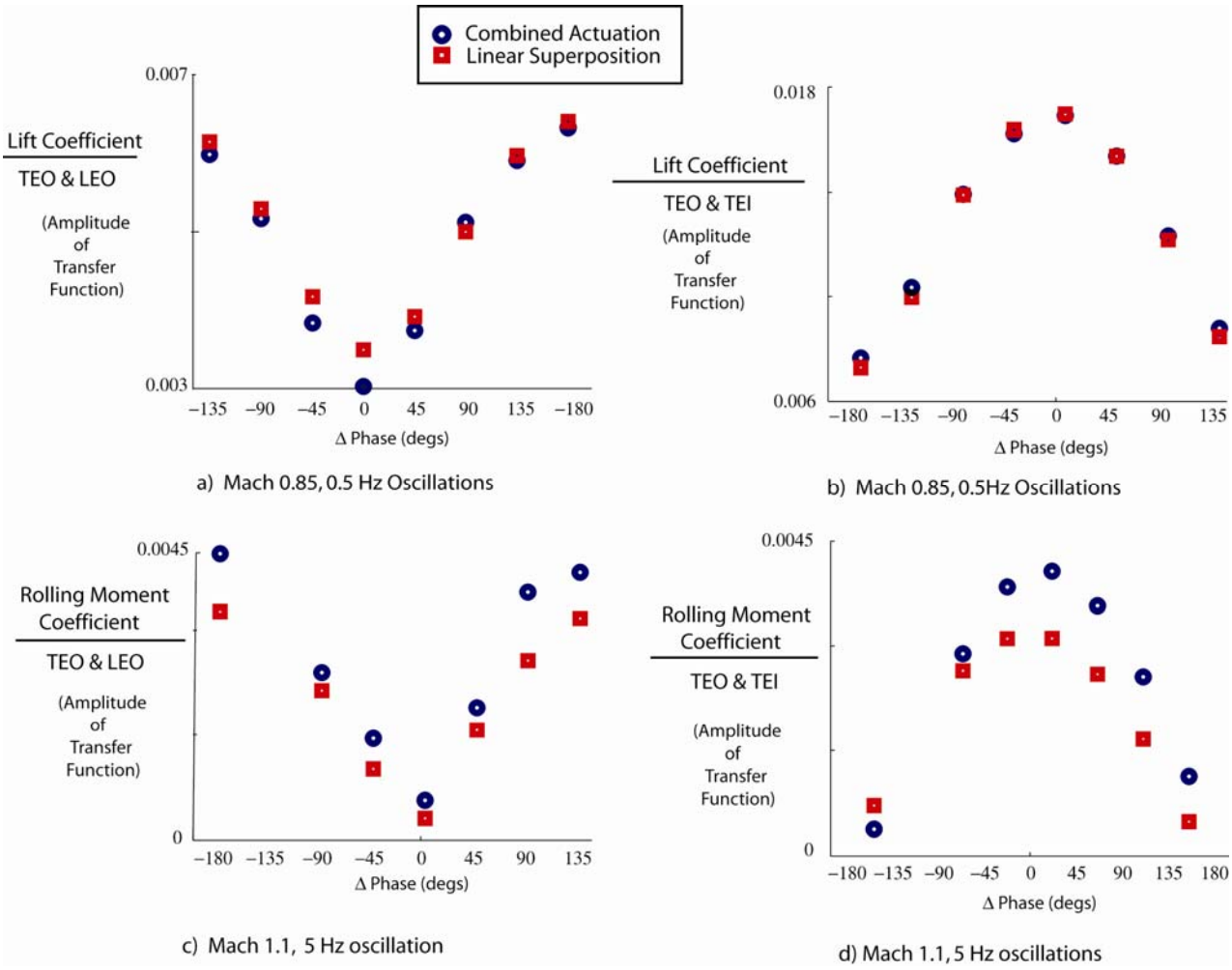

Figure 14. Transfer Function Amplitudes due to control surface oscillations at fixed frequencies

Linear superposition gives a good indication of the combined actuation response, provided that the phasing is correctly accounted for, in the cases of lift, rolling moment and root bending moment. This is true for each of the four pairings of control surfaces tested.

The response-maximizing phase angles are summarized in Table 3 for lift coefficient, rolling moment coefficient, and wing root bending moment. This information is also pertinent to the static data. In the data shown in figure 7, data sets 1 and 3 represent out-of-phase displacements of the TEO and LEO control surfaces. Note that the out-of-phase responses are generally larger than the in-phase response, shown in data sets 2 and 4.

There were 160 plots of amplitude versus phase generated from the different loads, control surface combinations, Mach numbers and frequencies of oscillations. Note that in each of the plots shown in figure 14, the amplitude is a clearly shaped function of phase angle. This characteristic is present for 100% of the linear superposition results generated and 83% of the simultaneous actuation results. This allows for general statements to be made regarding which combinations of control surface deflection produce minimum and maximum responses. All of the excepted results are pitching moment, yawing moment and outboard span station torsion moment.

Table 3 Control surface phase angles that maximize response

	TEO & LEO	TEI & LEI	TEO & TEI	LEO & LEI
Lift	***180°***	***0°***	***0°***	***0°***
Rolling Moment	***180°***	***0°***	***0°***	***0°***
Root Bending Moment	***180°***	***180°***	***0°***	***0°***

VI. Conclusions

Control surface interactions were investigated in both static control actuation testing and dynamic control surface oscillation testing. The primary method of evaluating interactions was examination of the goodness of the linear superposition assumptions. Responses produced by independently actuating single control surfaces were combined and compared with responses produced by simultaneously actuating multiple control surfaces. Adjustments to the data were required to isolate the control surface influences. Using dynamic data, the task increases, as both the amplitude and phase have to be considered in the data corrections.

Static control surface deflection data showed excellent agreement between the superposition results and the combined actuation results, for some of the data sets. These results considered combining the outboard control surfaces. The symmetric balance loads are well-captured using linear superposition of multiple control surfaces. The antisymmetric balance loads and wing bending loads are more poorly captured, but in some cases sufficiently represented. Accurate representation of wing torsion loads are not generated by combining individual control surface contributions. The results did not show a dramatic decrease in quality of the superposition assumption when the loads were measured in the vicinity of the control surface load paths.

Analysis of variance was used to assess which factors in the experiment significantly contributed to the errors produced. The test condition and changes to the hardware were found to have a more significant influence than the control surface phasing or amplitude.

Oscillatory control surface deflections were used to generate dynamic data. Analysis of the balance loads and the wing loads indicate that as the frequency of control surface oscillation increases the errors due to linear superposition generally increase. The largest superposition errors were observed not when combining all four control surfaces, but when combining tandem pairings (TEI & LEO or TEI & LEI).

The effectiveness of the control surfaces is highly dependent upon the phasing between those control surfaces. This is seen in both the static and dynamic data. For all control surface pairings, except LEO & TEO acting together, the effectiveness of combined control surface actuation is maximized when they act in-phase. Combining the LEO and TEO control surface deflections, the maximum responses are achieved when they act out-of-phase.

The transfer function data is generally characterized by a shaped function when the amplitude is plotted as a function of relative phase angle, with the maximum lying at either 0º or 180º. Linear superposition gives good representations of the curves with respect to relative phasing, particularly for the lift coefficient, rolling moment coefficient, and bending loads.

References

[1] Wilson, J.R., "A twisted approach to wing warping," Aerospace America, October 2005, Pages 28-31,42.

[2] Pendleton, E. W., Bessette, D., Field, P.B., Miller, G. D., and Griffin, K.E., "Active aeroelastic wing flight research program and model analytical development," AIAA Journal of Aircraft, Vol 37, No. 4, July-August 2000.

[3] Boehm, B., Flick, P., Sanders, B., Pettit, C., Reichenbach, E.Y., and Zillmer, S., "Static aeroelastic response predictions of the Active Aeroelastic Wing (AAW) flight research vehicle," *AIAA/ASME/ASCE/AHS/ASC Structures, Structural Dynamics and Materials Conference*, April 2001, Seattle, Washington, AIAA-2001-1372.

[4] Wieseman, C.D., Silva, W.A., Spain, C.V., and Heeg, J., "Transonic Small Disturbance and Linear Analysis for the Active Aeroelastic Wing Program," *46th AIAA/ASME/ASCE/AHS/ASC Structures, Structural Dynamics and Materials Conference*, April, 2005, Austin, Texas.

[5] Raveh, D.E., and Levy, Y., "CFD-Based Aeroelastic Response of an Active Aeroelastic Wing," *45th AIAA/ASME/ASCE/AHS/ASC Structures, Structural Dynamics and Materials Conference*, April 2004, Palm Springs, California.AIAA 2004-1515.

[6] Heeg, J., Spain, C.V., Florance, J.R., Wieseman, C.D., Ivanco, T.G., DeMoss, J.A., Wilva, W.A., Panetta, A., Lively, P., and Tumwa, V., "Experimental Results from the Active Aeroelastic Wing Wind Tunnel Test Program," *46th AIAA/ASME/ASCE/AHS/ASC Structures, Structural Dynamics and Materials Conference*, April, 2005, Austin, Texas.

[7] Miller, G.D., "Active Flexible Wing (AFW) Technology," Final Report, NA-87-1515L, Rockwell International, September 1987.

[8] Perry, B. III, Cole, S.R., and Miller, G.D., "Summary of an active flexible wing program," AIAA Journal of Aircraft, Vol 32, No 1, January-February 1995.

[9] Carlsson, M., "Control Surface Response of a Blended Wing Body Aeroelastic Wind Tunnel Model," AIAA Journal of Aircraft, Vol 42, No.3, May-June 2005.

[10] Burken, J.J., Lu, P. and Zhenglu, W., "Reconfigurable flight control designs with application to the X-33 vehicle," *AIAA Guidance, Navigation and Control Conference and Exhibit*, Portland, Oregon, AIAA-1999-4134.

[11] Bieniawski, S., Kroo, I., and Wolpert, D., "Flight Control with Distributed Effectors," *AIAA Guidance, Navigation and Control Conference and Exhibit*, San Francisco, California, 2005, AIAA-2005-6074.

[12] Heeg, J., McGowan, A., Crawley, E., and Lin, C., "The piezoelectric aeroelastic response tailoring investigation: a status report," *SPIE 1995 North American Conference on Smart Structures and Materials*, San Diego California, Feb-March 1995.

[13] DiStefano, J.J., III, Stubberud, A.R., and Williams, I.J., *Schaum's Outline of Theory and Problems of Feedback and Control Systems*, McGraw Hill Book Company, New York, 1967.

[14] Mukhopadhyay, V., Newsom, J.R., and Abel, I., "A Method for Obtaining Reduced-Order Control Laws for High-Order Systems Using Optimization Techniques," NASA TP1876, 1981.

[15] Buttrill, C., Bacon, B., Heeg, J., Houck, J., and Wood, D., "Simulation and Model Reduction for the Active Flexible Wing Program," AIAA Journal of Aircraft, Vol 32, No 1, Jan-Feb 1995.

[16] Montgomery, D.C., *Design and Analysis of Experiments*, 5th ed., John Wiley and Sons, New York, 1997, Chaps. 2, 3, 5, 8, 9.

[17] Breyfogle, F.W. III, *Implementing Six Sigma; Smarter Solutions Using Statistical Methods*, John Wiley and Sons, New York, 1999.

[18] *NIST/SEMATECH e-Handbook of Statistical Methods*, http://www.itl.nist.gov/div898/handbook/, [cited April 5, 2006].

[19] Soong, T.T., *Probabilistic Modeling and Analysis in Science and Engineering*, John Wiley and Sons, New York, 1981, Chaps. 9, 10.